
# Raman scattering mediated by neighboring molecules

Mathew D. Williams, David S. Bradshaw, and David L. Andrews

Citation: The Journal of Chemical Physics **144**, 174304 (2016); doi: 10.1063/1.4948366

View online: http://dx.doi.org/10.1063/1.4948366

View Table of Contents: http://scitation.aip.org/content/aip/journal/jcp/144/17?ver=pdfcov

Published by the AIP Publishing



# Raman scattering mediated by neighboring molecules

Mathew D. Williams, David S. Bradshaw, and David L. Andrews[a)]
*School of Chemistry, University of East Anglia, Norwich NR4 7TJ, United Kingdom*

(Received 10 March 2016; accepted 18 April 2016; published online 5 May 2016)

Raman scattering is most commonly associated with a change in vibrational state within individual molecules, the corresponding frequency shift in the scattered light affording a key way of identifying material structures. In theories where both matter and light are treated quantum mechanically, the fundamental scattering process is represented as the concurrent annihilation of a photon from one radiation mode and creation of another in a different mode. Developing this quantum electrodynamical formulation, the focus of the present work is on the spectroscopic consequences of electrodynamic coupling between neighboring molecules or other kinds of optical center. To encompass these nanoscale interactions, through which the molecular states evolve under the dual influence of the input light and local fields, this work identifies and determines two major mechanisms for each of which different selection rules apply. The constituent optical centers are considered to be chemically different and held in a fixed orientation with respect to each other, either as two components of a larger molecule or a molecular assembly that can undergo free rotation in a fluid medium or as parts of a larger, solid material. The two centers are considered to be separated beyond wavefunction overlap but close enough together to fall within an optical near-field limit, which leads to high inverse power dependences on their local separation. In this investigation, individual centers undergo a Stokes transition, whilst each neighbor of a different species remains in its original electronic and vibrational state. Analogous principles are applicable for the anti-Stokes case. The analysis concludes by considering the experimental consequences of applying this spectroscopic interpretation to fluid media; explicitly, the selection rules and the impact of pressure on the radiant intensity of this process.  [http://dx.doi.org/10.1063/1.4948366]

## I. INTRODUCTION

Raman scattering involving individual optical centers is a well-established molecular process used as a spectroscopic[1–3] and microscopic tool[4,5] with an ever-increasing range of applications, including surface-enhanced spectroscopy,[6–11] sensing,[12–14] the detection of environmental pollutants,[15,16] and identification of disease.[17] The theoretical basis for the underlying phenomenon is well-known and established with quantum electrodynamical techniques offering a particularly insightful means of formulation.[18] The concurrent annihilation and creation of a photon of two different radiation modes is involved, typically entailing some exchange in vibrational energy with the system and thereby corresponding to an inelastic process. For molecular systems, the change in energy may occur within individual molecules of a solid, or more commonly, in freely tumbling molecules of a fluid. To secure theoretical results applicable to fluid media, in particular, requires careful consideration of molecular motion and the fluctuating impact on the local environment of the active optical centers.[19]

The proximity of neighboring molecules has an electrodynamic influence that extends beyond the familiar heterogeneous broadening of spectral lines. Such an influence may modify the symmetry of the system in which the scattering occurs, and thus, allow previously forbidden electronic transitions to take place. For example, a transition between states of formally opposite parity, *gerade–ungerade*, may become allowed in a centrosymmetric molecule due to the symmetry-lowering presence of a nearby molecule. The precise form of electronic coupling between centers that has the capacity to accomplish such an effect can be accommodated by considering one or more virtual photon exchanges,[20–22] which thereby link the evolution in quantum state for the two particles. Here, we consider both single and double exchanges, and all associated quantum interferences that can lead to modifications of the rules governing fundamental single-center Raman transitions.

Previously, work has been done to accommodate a second center in terms of bimolecular cooperative Raman excitation—leading to sum frequency shifts in the spectrum of scattered light—the underlying mechanism being one in which one molecule annihilates a photon and its paired center creates the Raman photon with both molecules undergoing vibrational transition.[23] Utilizing methods detailed by Andrews *et al.*,[24] we now extend this earlier Raman study, focusing on the experimentally more significant likelihood in which just one of the pair becomes vibrationally excited. This analysis also entertains contributions involving the transfer of either one or two virtual photons between the optical centers during

a)david.andrews@physics.org

 

the course of the Raman scattering and also the relevant quantum interference term. In spite of the increased number of coupling events, a potentially experimentally significant result is obtainable for such a higher-order mechanism, since the overall process retains its linear dependence on laser intensity.

To expedite the analysis of Raman signals that arise from two-center nanoscale interactions, two realistic assumptions are applied: in each pairwise dipolar interaction, the two components are considered to be chemically different and held in a fixed orientation with respect to each other, displaced from each other by a distance equivalent to the near-field optical region. Due to the latter condition, it transpires that each virtual photon exchange can justifiably be represented by longitudinal field interactions for each optical center involved, i.e., in the near-field region.[20] For particles separated by a few nanometers, the higher order dependences on displacement $R$ can become significant, and accordingly, the process becomes more readily measureable. In the following investigation, the center that intercepts a photon of input radiation undergoes a change in vibrational energy (i.e., a Raman transition), while each neighboring molecule, notwithstanding its electrodynamic participation, returns to the electronic and vibrational state from which it began. For the purposes of the calculations presented, a Stokes transition has been assumed, although analogous principles hold for the anti-Stokes counterpart.

It will be apparent that additional electrodynamic light-matter interactions involving the molecule responsible for the Raman signal can lead to the invocation of different selection rules. This work offers a thorough exploration of mechanisms for which at least one transition will be active, leading to new characteristic lines in the Raman spectrum. Pertinent results are presented with regards to the optical symmetry requirements of the individual molecules.

In the following analysis, the first subsections introduce and define key parameters, concisely setting forth the well-established quantum treatment of the vibrational Raman process in order that the variations introduced by pair interactions can be most readily understood. Subsequent subsections accommodate further tiers of complexity: explicitly one and two virtual photon exchanges, respectively. At this juncture, we focus on the application of these spectroscopic techniques to fluid media, including the relevance of modified selection rules—with the appropriate symmetry analysis applied to an example system—and a consideration of pressure dependence. Finally, the context for this work is discussed with regard to a range of applications.

## II. ANALYSIS

### A. Theory for single-center Raman scattering

To begin, molecular quantum electrodynamics theory is deployed for analysis of the evolution of system states to fully encompass the progression in molecular and radiation states.[18] Representing the process by a series of Feynman diagrams offers a visualization for the process: Fig. 1 presents one of the two time-orderings that have to be accommodated

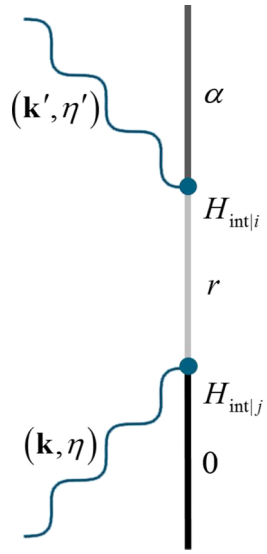


FIG. 1. One of the two Feynman diagrams for conventional Raman scattering by an isolated molecule (optical center). From the bottom upwards: a photon of wavevector $\mathbf{k}$ and polarization $\eta$ is annihilated and the molecule enters a virtual intermediate state $r$; subsequently, a photon of different wavevector $\mathbf{k}'$ and polarization $\eta'$ is created. Each interaction event, with associated Cartesian indices $i$ or $j$, engages a different component of the electric field operator in the interaction Hamiltonian, $H_{\text{int}}$. The overall change in energy of the radiation field is equivalent to that of the change in molecular states energy $E_\alpha - E_0$, where $\alpha$ relates to a vibrational excitation rather than an electronic one.

in the theory. By convention, the initial state is at the base and the final state at the top; in-between is a progression through virtual intermediate states. In the case of the fundamental (single-center) Raman scattering, the molecule begins in the ground state and undergoes two concerted photon events: one annihilation and one creation. The necessary molecule-field coupling is generally governed by the microscopic interaction Hamiltonian

$$H_{\text{int}} = -\frac{\boldsymbol{\mu} \cdot \mathbf{d}^{\perp}}{\varepsilon_0}, \tag{1}$$

in which $\boldsymbol{\mu}$ is the electric dipole operator for the molecule and $\mathbf{d}^{\perp}$ is the transverse electric field displacement operator at the appropriate location $\mathbf{r}$, as given by a radiation mode expansion

$$\mathbf{d}^{\perp}(\mathbf{r}) = i \sum_{\mathbf{k},\eta} \sqrt{\frac{\varepsilon_0 \hbar c k}{2V}} \left[ \mathbf{e}^{(\eta)}(\mathbf{k}) a^{(\eta)}(\mathbf{k}) \mathrm{e}^{i\mathbf{k}\cdot\mathbf{r}} - \bar{\mathbf{e}}^{(\eta)}(\mathbf{k}) a^{\dagger(\eta)}(\mathbf{k}) \mathrm{e}^{-i\mathbf{k}\cdot\mathbf{r}} \right], \tag{2}$$

where $\mathbf{e}^{(\eta)}$ is the polarization vector of the electric field, its complex conjugate denoted by an overbar, and $\eta$ denoting the polarization state; $a^{(\eta)}(\mathbf{k})$ and $a^{\dagger(\eta)}(\mathbf{k})$ are the corresponding photon annihilation and creation operators, respectively, for a given wavevector $\mathbf{k}$. Raman scattering involves photons of two relevant radiation states, one entering and one exiting the system: the pair has a disparity in energy corresponding to energy exchanges through the vibrational component of the molecule state, this is consistent with an inelastic scattering event.

Quantum mechanical principles demand summation over unobservable intermediate states. All eventualities leading

from the ground, 0, to the final state, $\alpha$, must be considered in the form of a summation over virtual molecular states, $r$. Moreover, there are two permutations for the ordering of photons to engage with the molecular state, the first as shown in Fig. 1; in its counterpart, the Raman photon creation precedes the input photon annihilation. The sum of the two corresponding terms gives the matrix element $M_{FI}$, which represents the complete Raman transition

$$M_{FI} = -\frac{\sqrt{kk'n}\hbar c}{2\varepsilon_0 V}\bar{e}'_i e_j \alpha^{\alpha 0}_{ij}. \tag{3}$$

Here, $V$ is the quantization volume, $n$ is the number of input photons each with energy $\hbar ck$ and polarization $\mathbf{e}$, the scattered photon parameters are signified by a prime, and $\alpha^{\alpha 0}_{ij}$ is the transition polarizability tensor, explicitly given by

$$\alpha^{\alpha 0}_{ij} = \sum_r \left\{ \frac{\mu^{\alpha r}_i \mu^{r0}_j}{E_{r0} - \hbar ck} + \frac{\mu^{\alpha r}_j \mu^{r0}_i}{E_{r0} + \hbar ck'} \right\}, \tag{4}$$

where both carry subscripts signifying Cartesian coordinates, taken for the present to refer specifically to the laboratory frame: indices $\{i, j, \ldots, n\}$ are used for this purpose here and henceforth. The above expression is composed of transition dipole moments connecting respective molecular states through $\mu^{\{\alpha,r\}\{r,0\}}_{\{i,j\}}$, and the Raman energy shift is determined from energy conservation arguments, which can be written as $E_\alpha - E_0 \equiv E_{\alpha 0} = \hbar ck - \hbar ck'$.

### B. Introducing the accommodation of neighbor interactions

At this stage, to anticipate the forthcoming development of terms that will accommodate pairwise neighbor interactions, the matrix element $M_{FI}$ is now supplemented by higher order terms still connecting the same initial and final states. These are to be written in a form that readily identifies the origin of each addendum. Terms in which the Raman-active molecule is singly coupled to a neighbor (see Fig. 2) are to be written in forms such as $M^{A'|B}_{FI}$; those involving two such couplings (see Fig. 3) in forms such as $M^{A'\|B}_{FI}$. The superscripts are to be interpreted as follows: $A$ is the molecule of spectroscopic interest, undergoing the Raman transition, and $B$ a local partner coupled to it by virtual photon exchange. The first letter of the superscript (read left-to-right) denotes the site of input photon annihilation; the number of solidi between the pair of letters denotes the number of virtual photons exchanged, and a prime is attached to the label for the molecule creating the photon. It will be shown that accommodating such effects still involves the same number of detectable photons and as such retains the usual linear dependence on the intensity of the laser beam input.

Collecting terms into their appropriate orders, the matrix elements are now deployed into a formula (related to Fermi's golden rule[25]), cast in terms of the input laser irradiance $I_0$, that determines the resultant observable: the radiant intensity, $I'$, for Raman emission into a solid angle $\Omega'$

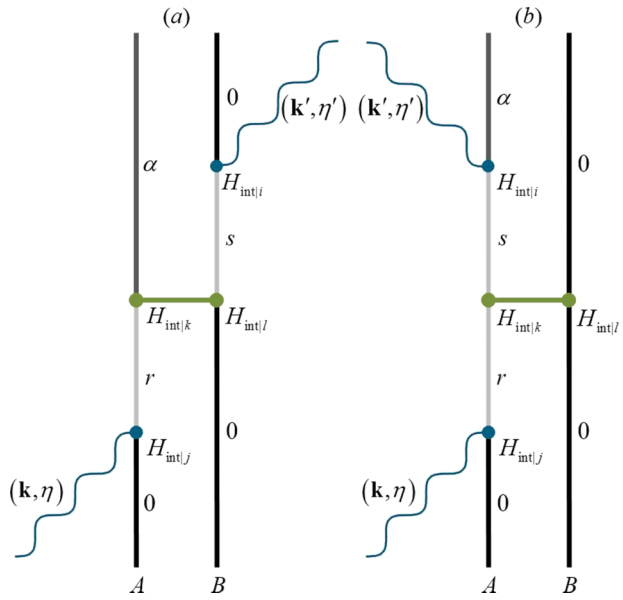


FIG. 2. Representative Feynman diagrams for the time evolution of molecules $A$ and $B$, the former undergoing a Raman transition, with the pair coupled by a virtual photon. The horizontal line depicts near-zone virtual photon exchange which, tending to the static limit, casts the coupling in a form equivalent to an instantaneous interaction. In each case, the coupling introduces a second intermediary state $s$ at one of the two molecules. The interaction series, made up of four interactions overall, is exhibited by (a) two interactions at both molecules $A$ and $B$; (b) three interactions at $A$ and one at $B$. In both cases, a full set of distinct time-orderings has to be accommodated in the theory.

$$I'(\Omega') = \left(\frac{k'^2}{4\pi\varepsilon_0}\right)^2 I_0 \times \Bigg| \underbrace{M_{FI}}_{0} + \underbrace{M^{A'|B}_{FI} + M^{B'|A}_{FI} + M^{A|B'}_{FI} + M^{B|A'}_{FI}}_{1} + \underbrace{M^{A'\|B}_{FI} + M^{B'\|A}_{FI} + M^{A\|B'}_{FI} + M^{B\|A'}_{FI}}_{2} + \cdots \Bigg|^2. \tag{5}$$

Here, the underbraces group the terms with order 0, 1, or 2, which correspond to the number of virtual photon(s) exchanged between molecules $A$ and $B$.

### C. Born-Oppenheimer development of the transition tensors

To proceed further, it is necessary to separate the nuclear and electronic wavefunctions in order to correctly represent the properties involved in the vibrational Raman transition. The procedure can be illustrated with reference to the simple transition polarizability tensor, as given by Equation (4), which features in both the conventional, single-center matrix elements, and also, as will emerge later, those for two-center Raman processes. It is well-known that the standard development leads to rate equations cast in terms of the derivative of the molecule polarizability with respect to each active vibration. The resulting rate terms are smaller in magnitude than those associated with the polarizability itself, as is apparent from the relative weakness of Raman

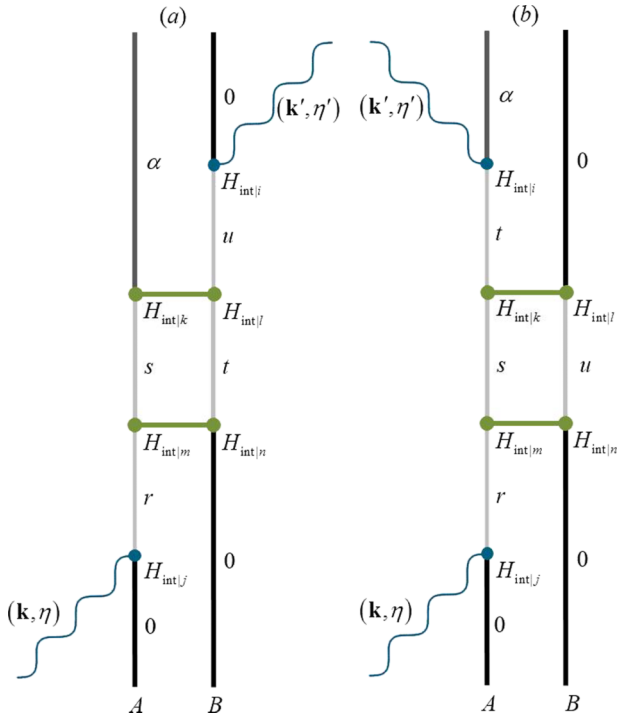


FIG. 3. Same as Fig. 2, except two virtual photon exchanges occur between molecules $A$ and $B$, resulting in a total of six interactions, namely: (a) three interactions at $A$ and $B$; (b) four interactions at $A$ and two at $B$. Additional intermediary states, $t$ and $u$, are assigned to either molecule.

compared to Rayleigh scattering. In the present analysis, we note that the processes of interest lead to vibrational mode expansions for only one of the two participating molecular centers; accordingly, the results are of much higher potential experimental significance than any instances of cooperative, dual vibrational excitation.[23]

Assuming validity of the Born-Oppenheimer approximation, each of the molecular states implicit in the transition moments is now written as a product of electronic and nuclear states, viz., $|\Psi_r(\{q\},\{Q\})\rangle \Rightarrow |\varphi_r(\{q\}|_Q)\rangle \prod_u \left|\psi^r_{R_u}(Q_u)\right\rangle$. Here, $\{q\}$ and $\{Q\}$, respectively, signify the sets of normal vibrational mode coordinates, and it is implicit that the electrons respond instantaneously to the nuclei. Thus, $\varphi_r$ designates an electronic wavefunction with a parametric dependence on the set of nuclear positions; $\psi_R$ is a vibrational wavefunction for level $R$. Also, $Q_u$ is the $u$th member of the set of nuclear coordinates for the normal modes of vibration, and $\psi^r_{R_u}$ specifically represents the wavefunction in a normal mode of simple harmonic vibration $u$ over the potential energy surface created by the electronic state $r$. For the Raman process of interest, the initial, intermediate, and final states in each term of the above equation can thus be cast as $|\varphi_0\rangle \prod_u \left|\psi^0_{0_u}\right\rangle; |\varphi_r\rangle \prod_u \left|\psi^r_{R_u}\right\rangle; |\varphi_0\rangle \prod_u \left|\psi^0_{\alpha_u}\right\rangle$, respectively. We now interpret each transition moment component as a Dirac bracket succinctly expressed as $\mu_i^{\alpha r} \Rightarrow \langle\psi_\alpha|\,\mu_i^{0r}\,|\psi_0\rangle$. Equally, each energy term separates into an electronic and a vibrational term, i.e., $E_{\alpha r} \Rightarrow E_{0r} + E_{\alpha R}$. [For convenience, we focus upon just one of the nuclear vibrational modes, assuming a fundamental transition that leaves other modes unchanged in energy; hence, we can drop the subscript $u$]. By accounting for these decompositions, Equation (4) now becomes

$$\alpha_{ij}^{\alpha 0} = \sum_{r,R}\left[\frac{\langle\psi_\alpha|\mu_i^{0r}(Q)|\psi_R\rangle\langle\psi_R|\mu_j^{r0}(Q)|\psi_0\rangle}{E_{r0}+E_{R0}-\hbar ck} + \frac{\langle\psi_\alpha|\mu_j^{0r}(Q)|\psi_R\rangle\langle\psi_R|\mu_i^{r0}(Q)|\psi_0\rangle}{E_{r0}+E_{R\alpha}+\hbar ck}\right], \tag{6}$$

where each transition moment component, such as $\mu_i$, clearly refers to a Cartesian laboratory frame and depends parametrically on the nuclear orientation. In the denominators, energy conservation has been deployed to cast the full result in a form depending solely on the magnitude of the wavevector $\mathbf{k}$, and hence the frequency of the input beam.

At this juncture, it is presumed that the relevant photon and electronic state energies will greatly exceed the vibrational energy differences, providing that the input optical frequency is far from resonance. On this basis, the following approximation is commonly justified:

$$\alpha_{ij}^{\alpha 0} \approx \sum_{r,R}\left[\frac{\langle\psi_\alpha|\mu_i^{0r}(Q)|\psi_R\rangle\langle\psi_R|\mu_j^{r0}(Q)|\psi_0\rangle}{E_{r0}-\hbar ck} + \frac{\langle\psi_\alpha|\mu_j^{0r}(Q)|\psi_R\rangle\langle\psi_R|\mu_i^{r0}(Q)|\psi_0\rangle}{E_{r0}+\hbar ck}\right]. \tag{7}$$

Since the denominators in Equation (7) do not involve vibrational state energies, the completeness relation can be invoked, i.e., $\mathbf{1} \equiv \sum_r |\psi_R\rangle\langle\psi_R|$, so that

$$\alpha_{ij}^{\alpha 0} \approx \langle\psi_\alpha| \underbrace{\sum_r\left[\frac{\mu_i^{0r}(Q)\,\mu_j^{r0}(Q)}{E_{r0}-\hbar ck} + \frac{\mu_j^{0r}(Q)\,\mu_i^{r0}(Q)}{E_{r0}+\hbar ck}\right]}_{\alpha_{ij}^{00}(Q)} |\psi_0\rangle\,. \tag{8}$$

As a result of the nuclear motions producing little variation in the transition moments, a Taylor series expansion can be deployed of the electronic polarizability $\alpha_{ij}^{00}$ in terms of the vibrational coordinate $Q$ about the equilibrium position $Q_0$

$$\alpha_{ij}^{00}(Q) = \alpha_{ij}^{00}\big|_{Q_0} + (Q-Q_0)\left.\frac{\partial\alpha_{ij}^{00}}{\partial Q}\right|_{Q_0} + \cdots. \tag{9}$$

Accordingly, by inserting Equation (9) into (8), the leading term of the transition polarizability emerges in the approximate form

$$\alpha_{ij}^{\alpha 0} \approx \langle\psi_\alpha|\,(Q-Q_0)\,|\psi_0\rangle \left.\frac{\partial\alpha_{ij}^{00}}{\partial Q}\right|_{Q_0} + \cdots. \tag{10}$$

The symmetry properties of the right-hand side in Equation (10) fundamentally determine the criteria for allowing a Raman transition to occur. For the Dirac bracket to be non-zero serves to ensure that the dominant transitions are those that involve one quantum of vibrational energy. Equally, the derivative of the dynamic polarizability with respect to any vibrational coordinate determines that only those polarizability tensor elements of the corresponding symmetry species are allowed. The appropriate irreducible representations are readily identified by the quadratic terms that are listed in most common character tables.[26] These

features will be further discussed following our analysis of two-center scattering events.

### D. Raman scattering with virtual photon coupling to a neighbor

Consider the presence of a second molecule in close proximity to molecule $A$, namely, the optical center that undergoes the Raman transition. As a result, we can find eight distinct mechanisms by means of which the Raman transition at $A$ occurs under the influence of a second optical center. The set of four that involve a single virtual photon exchange between the two molecules are first examined; these include (i) photon annihilation at $A$ and photon creation at $B$, denoted by $M_{FI}^{A|B'}$ and shown in Fig. 2(a); (ii) annihilation at $B$ and creation at $A$, signified by $M_{FI}^{B|A'}$; (iii) photon annihilation and creation at $A$, represented by $M_{FI}^{A'|B}$ and given in Fig. 2(b); and (iv) annihilation and creation at $B$, symbolized by $M_{FI}^{B'|A}$. Each case has six possible permutations, or time-orderings, of the interaction events; to obtain the formulations that follow, all must be considered. It is noteworthy, moreover, that energy exchange between molecules does *not* occur in case (iii), which is consistent with the requirement of a polar molecule $B$, but does arise for the other three situations.

In the near-zone region, the longitudinal contributions of the virtual photon with respect to the displacement $\mathbf{R}$ dominates,[27] and the matrix elements corresponding to cases (i) and (ii) can be written in a simplified form

$$M_{FI}^{A|B'} = \frac{\sqrt{kk'n}\hbar c}{8\pi\varepsilon_0^2 V} R^{-3}\overline{e}_i' e_j \left(\delta_{kl} - 3\hat{R}_k\hat{R}_l\right) \alpha_{jk}'^{\alpha 0|A} \alpha_{il}''^{00|B}, \quad (11)$$

$$M_{FI}^{B|A'} = \frac{\sqrt{kk'n}\hbar c}{8\pi\varepsilon_0^2 V} R^{-3}\overline{e}_i' e_j \left(\delta_{kl} - 3\hat{R}_k\hat{R}_l\right) \alpha_{jk}'^{00|B} \alpha_{il}''^{\alpha 0|A}, \quad (12)$$

where short-range coupling tensor $\mathbf{V}$ has been employed[20] and the explicit form of the polarizabilities $\alpha_{jk}'$ and $\alpha_{il}''$, relating to the two photon interaction at either molecule, is given by[23]

$$\alpha_{jk}'^{\alpha 0|A} = 2\sum_r \left\{ \frac{\mu_k^{\alpha r|A}\mu_j^{r0|A}}{E_{r0}^A - \hbar ck} + \frac{\mu_j^{\alpha r|A}\mu_k^{r0|A}}{E_{r0}^A + \hbar ck'} \right\}, \quad (13)$$

$$\alpha_{il}''^{00|B} = 2\sum_s \left\{ \frac{\mu_i^{0s|B}\mu_l^{s0|B}}{E_{s0}^B - \hbar ck'} + \frac{\mu_l^{0s|B}\mu_i^{s0|B}}{E_{s0}^B + \hbar ck'} \right\}. \quad (14)$$

In contrast, cases (iii) and (iv) invoke a three-photon interaction at one molecule and a single one at the other, so that the respective tensors $\beta_{ijk}$ (transition hyperpolarizability) and $\mu_l$ (dipole) are engaged to obtain

$$M_{FI}^{A'|B} = \frac{\sqrt{kk'n}\hbar c}{8\pi\varepsilon_0^2 V} R^{-3}\overline{e}_i' e_j \left(\delta_{kl} - 3\hat{R}_k\hat{R}_l\right) \beta_{ijk}^{\alpha 0|A}\mu_l^{00|B}, \quad (15)$$

$$M_{FI}^{B'|A} = \frac{\sqrt{kk'n}\hbar c}{8\pi\varepsilon_0^2 V} R^{-3}\overline{e}_i' e_j \left(\delta_{kl} - 3\hat{R}_k\hat{R}_l\right) \beta_{ijk}^{00|B}\mu_l^{\alpha 0|A}. \quad (16)$$

In the former, Equation (15), $\mu_l^{00|B}$ denotes a permanent static dipole (i.e., $B$ is required to be a polar molecule), and the transition hyperpolarizability is given by

$$\beta_{ijk}^{\alpha 0|A} = \sum_{r,s} \left\{ \frac{\mu_i^{\alpha s|A}\mu_k^{sr|A}\mu_j^{r0|A}}{\left[E_{s0}^A - \hbar ck\right]\left[E_{r0}^A - \hbar ck\right]} + \cdots \right\} \quad (17)$$

(see Equation (S1) in the supplementary material for the complete six term form of this expression[28]). Again, using the Born-Oppenheimer approximation and securing a result from a Taylor series expansion, a similar expression to Equation (9) for $\alpha_{ij}^{\alpha 0}$ is found

$$\beta_{ijk}^{\alpha 0} \approx \left\langle \psi_\beta \left| (Q - Q_0) \right| \psi_0 \right\rangle \left. \frac{\partial \beta_{ijk}^{00}}{\partial Q} \right|_{Q_0} + \cdots. \quad (18)$$

Here, $\beta_{ijk}^{00|B} \equiv \beta_{ijk}^{00|B}(-k';k,0)$ involves the vibration-induced displacements of the ground state property tensor with a structure analogous to the linear electro-optic tensor.[29] Such a hyperpolarizability tensor leads to vibrational selection rules relating to a three-photon process, directly identifiable in practice with those that apply to hyper-Raman spectroscopy. In point group tables, the corresponding allowed irreducible representations are those denoted by cubic terms found in more in-depth character tables.[26]

Conversely, in the above Equation (16), where the hyperpolarizability features directly in the form of a ground state dynamic property tensor, it is the dipole moment that exhibits the effects of vibration-induced displacements, leading to the same selection rules as infrared absorption.

### E. Raman scattering with coupling of two virtual photons to a neighbor

Now consider the second set of four processes (introduced in Subsection II D), which involve two virtual photon exchanges between $A$ and $B$. These new cases (v)-(viii) are, respectively, identical to the previous scenarios (i)-(iv), except for the inclusion of the additional virtual photon. Each process has twelve possible permutations, and none of them requires the involvement of a polar molecule. Figs. 3(a) and 3(b) display indicative Feynman diagrams that depict cases (v) and (vii), respectively, represented by $M_{FI}^{A\|B'}$ and $M_{FI}^{A'\|B}$ in the following formulas.

In the near-zone region, the matrix elements that correspond to cases (vii) and (viii) are written as

$$M_{FI}^{A'\|B} = -\frac{\sqrt{kk'n}\hbar c}{32\pi^2\varepsilon_0^3 V} R^{-6}\overline{e}_i' e_j \left(\delta_{kl} - 3\hat{R}_k\hat{R}_l\right) \times \left(\delta_{mn} - 3\hat{R}_m\hat{R}_n\right) \chi_{ijkm;ln}^{\alpha 0|A;00|B}, \quad (19)$$

$$M_{FI}^{B'\|A} = -\frac{\sqrt{kk'n}\hbar c}{32\pi^2\varepsilon_0^3 V} R^{-6}\overline{e}_i' e_j \left(\delta_{kl} - 3\hat{R}_k\hat{R}_l\right) \times \left(\delta_{mn} - 3\hat{R}_m\hat{R}_n\right) \chi_{ijkm;ln}^{00|B;\alpha 0|A}. \quad (20)$$

Here, with the extra complexity resulting from inclusion of the second virtual photon, the relevant tensors cannot be split into two and assigned to molecules $A$ and $B$ (as previously). Therefore, the $\chi$ tensors of Equations (19) and (20) include a mixture of features from both molecules, which is explicitly written as

$$\chi^{\alpha 0|A;00|B}_{ijkm;ln} = \sum_{r,s,t,u} \left\{ \frac{\mu^{\alpha t|A}_i \mu^{ts|A}_k \mu^{sr|A}_m \mu^{r0|A}_j \mu^{0u|B}_l \mu^{u0|B}_n}{\left[E^A_{t0} - \hbar c k\right]\left[E^A_{s0} + E^B_{u0} - \hbar c k\right]\left[E^A_{r0} - \hbar c k\right]} + \cdots \right\}, \tag{21}$$

and $\chi^{00|B;\alpha 0|A}_{ijkm;ln}$ is obtained by simply interchanging $A$ and $B$. The complete twelve-term form of the tensor is displayed in the supplementary material as Equation (S2).[28]

Despite it not being possible to factorize Equation (21) to obtain separate features associated with molecules $A$ and $B$, the selection rules and symmetry arguments can be applied to each numerator (which suffer no such limitation). Since the latter all involve four dipole moments on molecule $A$ and two on $B$, it is apparent that the entirety of the tensor expression relates to four-photon selection rules for $A$ and two-photon rules for $B$. For example, the numerator of the first term of Equation (21) relating to $A$ given by

$$C^{(1)}_{ikmj}(Q) = \mu^{\alpha t|A}_i(Q)\,\mu^{ts|A}_k(Q)\,\mu^{sr|A}_m(Q)\,\mu^{r0|A}_j(Q), \tag{22}$$

where the $Q$-dependence is now explicit (for a specific vibration) and is associated with the four-photon rules. To apply the Born-Oppenheimer approximation to this mechanism, it is necessary to consider each term individually, so the above example will produce

$$C^{(1)\,\alpha 0}_{ikmj}(Q) \approx \langle \psi_C |(Q - Q_0)| \psi_0 \rangle \left.\frac{\partial C^{(1)\,00}_{ikmj}}{\partial Q}\right|_{Q_0} + \cdots, \tag{23}$$

which is the first term of a set of twelve.

Returning to cases (v) and (vi), the corresponding matrix elements are now cast as

$$M^{A\|B'}_{FI} = -\frac{\sqrt{kk'n}\hbar c}{32\pi^2\varepsilon_0^3 V} R^{-6} \bar{e}'_i e_j \left(\delta_{kl} - 3\hat{R}_k\hat{R}_l\right) \times \left(\delta_{mn} - 3\hat{R}_m\hat{R}_n\right) \chi'^{\alpha 0|A;00|B}_{jkm;iln}, \tag{24}$$

$$M^{B\|A'}_{FI} = -\frac{\sqrt{kk'n}\hbar c}{32\pi^2\varepsilon_0^3 V} R^{-6} \bar{e}'_i e_j \left(\delta_{kl} - 3\hat{R}_k\hat{R}_l\right) \times \left(\delta_{mn} - 3\hat{R}_m\hat{R}_n\right) \chi'^{00|B;\alpha 0|A}_{jkm;iln}, \tag{25}$$

with the molecular response tensor given by

$$\chi'^{\alpha 0|A;00|B}_{jkm;iln} = \sum_{r,s,t,u} \left\{ \frac{\mu^{\alpha s|A}_k \mu^{sr|A}_m \mu^{r0|A}_j \mu^{0u|B}_i \mu^{ut|B}_l \mu^{t0|B}_n}{\left[E^B_{u0} - \hbar c k'\right]\left[E^A_{s0} + E^B_{t0} - \hbar c k\right]\left[E^A_{r0} - \hbar c k\right]} + \cdots \right\}. \tag{26}$$

The eleven successive terms appear in the supplementary material as Equation (S3).[28] Similar to Equation (22), the numerator of the first term of Equation (26) is defined as

$$C'^{(1)}_{kmj}(Q) = \mu^{\alpha s|A}_k(Q)\,\mu^{sr|A}_m(Q)\,\mu^{r0|A}_j(Q), \tag{27}$$

which corresponds to the three-photon selection rules at molecule $A$, and using the Born-Oppenheimer approximation, the resulting expression

$$C'^{(1)\,\alpha 0}_{kmj}(Q) \simeq \langle \psi_{C'} |(Q - Q_0)| \psi_0 \rangle \left.\frac{\partial C'^{(1)\,00}_{kmj}}{\partial Q}\right|_{Q_0} + \cdots. \tag{28}$$

This again is the explicit exemplar of a full set of twelve such terms, each subject to the same vibrational symmetry conditions.

### F. Scattering in fluid media

In Subsections II A–II E, our analysis has centered upon configurations where the molecules are set in fixed orientations, representing areas of application that are typically associated with molecules within a solid. More common are systems where the molecules are free to tumble within a condensed phase fluid, which will now be the subject of this and Subsections II G and II H. In the presented processes, it is reasonable to assume that the interacting molecules are fixed with respect to each other but free to rotate as a coupled molecular pair. This is justified on two grounds: (i) on the ultrafast time scale of the virtual photon(s) exchange the molecular pair is unable to reorient with respect to each other; (ii) in most systems where the molecules are held in close proximity, it is usually the case that there will be a preferred mutual orientation (i.e., a heavily weighted distribution). Therefore, the rotational average (to which the current section constitutes) is applied to the pair and not each individual molecule, i.e., the axial frame of reference of the molecular pair will be decoupled from the laboratory frame.

To begin, the explicit form of the matrix elements given by (3), (11), (12), (15), (16), (19), (20), (24), and (25) are inserted into Equation (5) for the radiant intensity, $I'$, producing an expression in which the matrix elements are multiplied by their complex conjugates and cross terms occur denoting quantum interference. The resulting 45-term expression then undergoes a 4th rank isotropic rotational-average, which can be described by the following tensor expression[30]

$$I^{(4)}_{ijop;\lambda\mu\nu\pi} = \frac{1}{30} \begin{pmatrix} \delta_{ij}\delta_{op} \\ \delta_{io}\delta_{jp} \\ \delta_{ip}\delta_{jo} \end{pmatrix}^{\mathrm{T}} \begin{pmatrix} 4 & -1 & -1 \\ -1 & 4 & -1 \\ -1 & -1 & 4 \end{pmatrix} \begin{pmatrix} \delta_{\lambda\mu}\delta_{\nu\pi} \\ \delta_{\lambda\nu}\delta_{\mu\pi} \\ \delta_{\lambda\pi}\delta_{\mu\nu} \end{pmatrix} = \sum_{r,s} f^{(4)}_r m^{(4)}_{rs} g^{(4)}_s, \tag{29}$$

where the elements of $f_r^{(4)}$ are identified with the three distinct isomers of the rank-4 isotropic tensor in the laboratory frame (denoted by Latin indices), $m_{rs}^{(4)}$ is the collective numerical coefficients, and $g_s^{(4)}$ denotes the three analogous rank-4 isotropic tensor isomers that are in the molecular frame (Greek indices). The polarizations associated with the incident and scattered light are identical in each term, and hence, the relevant part of the 45 terms determined from Equation (5) is treated similarly; the following common factor is thus obtained[31]

$$\bar{e}'_i e_j e'_o \bar{e}_p \begin{pmatrix} \delta_{ij}\delta_{op} \\ \delta_{io}\delta_{jp} \\ \delta_{ip}\delta_{jo} \end{pmatrix}^{\mathrm{T}} = \begin{pmatrix} |(\bar{\mathbf{e}}' \cdot \mathbf{e})|^2 \\ (\bar{\mathbf{e}}' \cdot \mathbf{e}')\,(\mathbf{e} \cdot \bar{\mathbf{e}}) \\ |(\mathbf{e} \cdot \mathbf{e}')|^2 \end{pmatrix}^{\mathrm{T}}. \tag{30}$$

At this juncture, using a standard right-angled scattering configuration, two conventional polarization schemes can be chosen: the electric field polarization of the scattered light is parallel or perpendicular to the incident light (schematically depicted by Figs. 4(a) and 4(b), respectively), as often employed in measuring a depolarization ratio.[32]

By adopting these two polarization schemes, numerical results can be obtained from Equation (30) and contracted with the numerical matrix, $m_{rs}^{(4)}$, in Equation (29). Therefore,

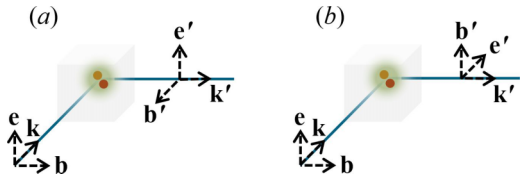


FIG. 4. Experimental setup: (a) parallel plane-polarized light is detected at right angles to the input laser; (b) perpendicularly plane-polarized light detected at right angles.

the parallel configuration produces the expression

$$\boldsymbol{P} = \frac{1}{15}\begin{pmatrix} 1 & 1 & 1 \end{pmatrix}, \tag{31}$$

and the perpendicular equivalent yields

$$\boldsymbol{P} = \frac{1}{30}\begin{pmatrix} -1 & 4 & -1 \end{pmatrix}. \tag{32}$$

These expressions are to be contracted with the molecular response tensors formed out of $g_s^{(4)}$ seen in Equation (29) along with the molecular response tensors $\{\alpha, \alpha', \alpha'', \beta, \chi, \chi'\}$ from the product of the appropriate matrix elements, to form a new complementary tensor now defined as $\boldsymbol{T}_w$, to appear in the following final result

$$\langle I'(\Omega')\rangle = \left(\frac{k'^2}{4\pi\varepsilon_0}\right)^2 I_0 \boldsymbol{P} \sum_{w=0}^{4} \left\{ \boldsymbol{T}_w \left(\frac{-1}{4\pi\varepsilon_0 R^3}\right)^w \prod_{q=1}^{w} \left(\delta_{\rho_q\sigma_q} - 3\hat{R}_{\rho_q}\hat{R}_{\sigma_q}\right) \right\}. \tag{33}$$

In Equation (33), the column vectors $\boldsymbol{T}_{\{0-4\}}$ signify rotational invariants formed from products of the Raman and associated transition tensors. The first of this set comprises the three scalar quantities that arise in conventional Raman scattering

$$\boldsymbol{T}_0 = \begin{pmatrix} \alpha^{\alpha 0|A}_{\lambda\lambda}\overline{\alpha}^{\alpha 0|A}_{\nu\nu} \\ \alpha^{\alpha 0|A}_{\lambda\mu}\overline{\alpha}^{\alpha 0|A}_{\lambda\mu} \\ \alpha^{\alpha 0|A}_{\lambda\mu}\overline{\alpha}^{\alpha 0|A}_{\mu\lambda} \end{pmatrix}. \tag{34}$$

The remaining invariants, $\boldsymbol{T}_{\{1-4\}}$, each hold a dependence on $\rho_{q,q+1,\ldots,w}$ and $\sigma_{q,q+1,\ldots,w}$ complementary with the parenthesis seen at the end of Equation (33). For example, the first instance can be seen here

$$\boldsymbol{T}_1 = \begin{pmatrix} \alpha^{\alpha 0|A}_{\lambda\lambda}\overline{\beta}^{\alpha 0|A}_{\nu\nu\rho_1}\overline{\mu}^{00|B}_{\sigma_1} \\ \alpha^{\alpha 0|A}_{\lambda\mu}\overline{\beta}^{\alpha 0|A}_{\lambda\mu\rho_1}\overline{\mu}^{00|B}_{\sigma_1} \\ \alpha^{\alpha 0|A}_{\lambda\mu}\overline{\beta}^{\alpha 0|A}_{\mu\lambda\rho_1}\overline{\mu}^{00|B}_{\sigma_1} \end{pmatrix} + \begin{pmatrix} \alpha^{\alpha 0|A}_{\lambda\lambda}\overline{\beta}^{00|B}_{\nu\nu\rho_1}\overline{\mu}^{\alpha 0|A}_{\sigma_1} \\ \alpha^{\alpha 0|A}_{\lambda\mu}\overline{\beta}^{00|B}_{\lambda\mu\rho_1}\overline{\mu}^{\alpha 0|A}_{\sigma_1} \\ \alpha^{\alpha 0|A}_{\lambda\mu}\overline{\beta}^{00|B}_{\mu\lambda\rho_1}\overline{\mu}^{\alpha 0|A}_{\sigma_1} \end{pmatrix}$$
$$+ \begin{pmatrix} \alpha^{\alpha 0|A}_{\lambda\lambda}\overline{\alpha}'^{\alpha 0|A}_{\nu\rho_1}\overline{\alpha}''^{00|B}_{\nu\sigma_1} \\ \alpha^{\alpha 0|A}_{\lambda\mu}\overline{\alpha}'^{\alpha 0|A}_{\lambda\rho_1}\overline{\alpha}''^{00|B}_{\mu\sigma_1} \\ \alpha^{\alpha 0|A}_{\lambda\mu}\overline{\alpha}'^{\alpha 0|A}_{\mu\rho_1}\overline{\alpha}''^{00|B}_{\lambda\sigma_1} \end{pmatrix} + \begin{pmatrix} \alpha^{\alpha 0|A}_{\lambda\lambda}\overline{\alpha}'^{00|B}_{\nu\rho_1}\overline{\alpha}''^{\alpha 0|A}_{\nu\sigma_1} \\ \alpha^{\alpha 0|A}_{\lambda\mu}\overline{\alpha}'^{00|B}_{\lambda\rho_1}\overline{\alpha}''^{\alpha 0|A}_{\mu\sigma_1} \\ \alpha^{\alpha 0|A}_{\lambda\mu}\overline{\alpha}'^{00|B}_{\mu\rho_1}\overline{\alpha}''^{\alpha 0|A}_{\lambda\sigma_1} \end{pmatrix}. \tag{35}$$

Each pair parentheses houses the appropriate set of molecular transition tensors for each pairwise product of matrix elements arising from Equation (5): $\boldsymbol{T}_2$, $\boldsymbol{T}_3$, and $\boldsymbol{T}_4$ are presented as Equations (S4), (S5), and (S6), respectively, in the supplementary material.[28]

### G. Exemplary systems

The range of applications for the above analysis is extensive, with broader aspects to be discussed in the concluding section. Here, we provide an illustration of a specific molecular system that can exemplify some of the symmetry issues. We shall consider an example where the molecule $A$ undergoing the Raman transition is benzene whose symmetry is consistent with the point group $D_{6h}$. Standard use of group theory tables readily reveals that for the normally Raman-forbidden transitions involving planar deformation vibrations of $B_{2g}$ symmetry, for example, Equation (26) becomes

$$\boldsymbol{T}_0, \boldsymbol{T}_1, \boldsymbol{T}_2 = 0, \tag{36}$$

$$\boldsymbol{T}_3 = \begin{pmatrix} \beta^{\alpha 0|A}_{\lambda\lambda\rho_1}\mu^{00|B}_{\sigma_1}\overline{\chi}'^{\alpha 0|A;00|B}_{\nu\rho_2\rho_3;\nu\sigma_2\sigma_3} \\ \beta^{\alpha 0|A}_{\lambda\mu\rho_1}\mu^{00|B}_{\sigma_1}\overline{\chi}'^{\alpha 0|A;00|B}_{\mu\rho_2\rho_3;\lambda\sigma_2\sigma_3} \\ \beta^{\alpha 0|A}_{\lambda\mu\rho_1}\mu^{00|B}_{\sigma_1}\overline{\chi}'^{\alpha 0|A;00|B}_{\lambda\rho_2\rho_3;\mu\sigma_2\sigma_3} \end{pmatrix} + \begin{pmatrix} \alpha'^{\alpha 0|A}_{\lambda\rho_1}\alpha''^{00|B}_{\lambda\sigma_1}\overline{\chi}'^{\alpha 0|A;00|B}_{\nu\rho_2\rho_3;\nu\sigma_2\sigma_3} \\ \alpha'^{\alpha 0|A}_{\mu\rho_1}\alpha''^{00|B}_{\lambda\sigma_1}\overline{\chi}'^{\alpha 0|A;00|B}_{\mu\rho_2\rho_3;\lambda\sigma_2\sigma_3} \\ \alpha'^{\alpha 0|A}_{\mu\rho_1}\alpha''^{00|B}_{\lambda\sigma_1}\overline{\chi}'^{\alpha 0|A;00|B}_{\lambda\rho_2\rho_3;\mu\sigma_2\sigma_3} \end{pmatrix} + \begin{pmatrix} \chi'^{\alpha 0|A;00|B}_{\lambda\rho_1\rho_2;\lambda\sigma_1\sigma_2}\overline{\beta}^{00|B}_{\nu\nu\rho_3}\overline{\mu}^{\alpha 0|A}_{\sigma_3} \\ \chi'^{\alpha 0|A;00|B}_{\mu\rho_1\rho_2;\lambda\sigma_1\sigma_2}\overline{\beta}^{00|B}_{\lambda\mu\rho_3}\overline{\mu}^{\alpha 0|A}_{\sigma_3} \\ \chi'^{\alpha 0|A;00|B}_{\mu\rho_1\rho_2;\lambda\sigma_1\sigma_2}\overline{\beta}^{00|B}_{\mu\lambda\rho_3}\overline{\mu}^{\alpha 0|A}_{\sigma_3} \end{pmatrix}$$
$$+ \begin{pmatrix} \chi'^{\alpha 0|A;00|B}_{\lambda\rho_1\rho_2;\lambda\sigma_1\sigma_2}\overline{\alpha}'^{00|B}_{\nu\rho_3}\overline{\alpha}''^{\alpha 0|A}_{\nu\sigma_3} \\ \chi'^{\alpha 0|A;00|B}_{\mu\rho_1\rho_2;\lambda\sigma_1\sigma_2}\overline{\alpha}'^{00|B}_{\lambda\rho_3}\overline{\alpha}''^{\alpha 0|A}_{\mu\sigma_3} \\ \chi'^{\alpha 0|A;00|B}_{\mu\rho_1\rho_2;\lambda\sigma_1\sigma_2}\overline{\alpha}'^{00|B}_{\mu\rho_3}\overline{\alpha}''^{\alpha 0|A}_{\lambda\sigma_3} \end{pmatrix}, \tag{37}$$

$$\boldsymbol{T}_4 = \begin{pmatrix} \chi^{\alpha 0|A;00|B}_{\lambda\lambda\rho_1\rho_2;\sigma_1\sigma_2}\overline{\chi}'^{\alpha 0|A;00|B}_{\nu\rho_3\rho_4;\nu\sigma_3\sigma_4} \\ \chi^{\alpha 0|A;00|B}_{\lambda\mu\rho_1\rho_2;\sigma_1\sigma_2}\overline{\chi}'^{\alpha 0|A;00|B}_{\mu\rho_3\rho_4;\lambda\sigma_3\sigma_4} \\ \chi^{\alpha 0|A;00|B}_{\lambda\mu\rho_1\rho_2;\sigma_1\sigma_2}\overline{\chi}'^{\alpha 0|A;00|B}_{\lambda\rho_3\rho_4;\mu\sigma_3\sigma_4} \end{pmatrix} + \begin{pmatrix} \chi'^{\alpha 0|A;00|B}_{\lambda\rho_1\rho_2;\lambda\sigma_1\sigma_2}\overline{\chi}'^{\alpha 0|A;00|B}_{\nu\rho_3\rho_4;\nu\sigma_3\sigma_4} \\ \chi'^{\alpha 0|A;00|B}_{\mu\rho_1\rho_2;\lambda\sigma_1\sigma_2}\overline{\chi}'^{\alpha 0|A;00|B}_{\mu\rho_3\rho_4;\lambda\sigma_3\sigma_4} \\ \chi'^{\alpha 0|A;00|B}_{\mu\rho_1\rho_2;\lambda\sigma_1\sigma_2}\overline{\chi}'^{\alpha 0|A;00|B}_{\lambda\rho_3\rho_4;\mu\sigma_3\sigma_4} \end{pmatrix} + \begin{pmatrix} \chi'^{\alpha 0|A;00|B}_{\lambda\rho_1\rho_2;\lambda\sigma_1\sigma_2}\overline{\chi}'^{00|B;\alpha 0|A}_{\nu\rho_3\rho_4;\nu\sigma_3\sigma_4} \\ \chi'^{\alpha 0|A;00|B}_{\mu\rho_1\rho_2;\lambda\sigma_1\sigma_2}\overline{\chi}'^{00|B;\alpha 0|A}_{\mu\rho_3\rho_4;\lambda\sigma_3\sigma_4} \\ \chi'^{\alpha 0|A;00|B}_{\mu\rho_1\rho_2;\lambda\sigma_1\sigma_2}\overline{\chi}'^{00|B;\alpha 0|A}_{\lambda\rho_3\rho_4;\mu\sigma_3\sigma_4} \end{pmatrix}$$
$$+ \begin{pmatrix} \chi'^{\alpha 0|A;00|B}_{\lambda\rho_1\rho_2;\lambda\sigma_1\sigma_2}\overline{\chi}^{00|B;\alpha 0|A}_{\nu\nu\rho_3\rho_4;\sigma_3\sigma_4} \\ \chi'^{\alpha 0|A;00|B}_{\mu\rho_1\rho_2;\lambda\sigma_1\sigma_2}\overline{\chi}^{00|B;\alpha 0|A}_{\lambda\mu\rho_3\rho_4;\sigma_3\sigma_4} \\ \chi'^{\alpha 0|A;00|B}_{\mu\rho_1\rho_2;\lambda\sigma_1\sigma_2}\overline{\chi}^{00|B;\alpha 0|A}_{\mu\lambda\rho_3\rho_4;\sigma_3\sigma_4} \end{pmatrix}. \tag{38}$$

Further inspection of the tensor structures in the above non-zero results indicates that terms involving three-photon interactions by molecule $A$ (which would follow hyper-Raman or "cubic" selection rules) will also be forbidden. However, all other terms connected with two-photon ("quadratic") or four-photon ("quartic") interactions will be allowed. The result is a weak Raman signal with a depolarization ratio that is not constrained to the usual $[0, 3/4]$ range associated with non-resonant Raman signals.[33]

### H. Pressure dependence of the rate of scattering

Finally, it is possible to identify within the Raman spectrum the effects of pressure within the system. The range at which the virtual photon exchange occurs has an effect on the level to which the pressure impacts the spectrum. In order to pin down the precise pressure dependence, we must consider the density dependence of the pair correlation function for the fluid, as well as the dependence on molecular separation $R$ in each contributing process.

It is known that conventional Raman scattering in the condensed phase produces signals whose weak intensity variation with pressure, $\Delta I'$ (in the absence of phase changes) generally relates to the bulk isothermal compressibility $\beta_T$ as $\Delta I' \propto \beta_T$. This simply reflects the proportionately larger number of scatterers intercepted by the laser input beam when the effective volume per molecule becomes diminished. Correlated two-center scattering events might be anticipated to depend quadratically upon the compressibility, but in the present analysis, we also have to account for single- and two-center quantum interference terms. Moreover, in the cases we have examined, the electrodynamic coupling introduces an additional dependence through the $R^{-3w}$ factor in the $\boldsymbol{T}_w$ tensors featured in Equation (33). The overall consequence is that the intensities of lines that specifically derive from pair coupling will be associated with a nonlinear compressibility dependence

$$\Delta I'(T_w) \propto \beta_T^n, \quad (w > 0) \tag{39}$$

with the power $n$ in the range $[2.5 \leq n \leq 6]$. The sharp nonlinearity should make the detection of such lines through pressure-dependent studies especially identifiable, for example, through log-log plots of intensity against pressure.

## III. DISCUSSION

From the presented analysis, it is apparent that there are two distinct kinds of effect in Raman spectra that are readily identifiable as manifestations of local pairwise interactions. The first is a change in the intensity of conventional Raman-allowed lines, which arise from vibrational transitions associated with two-photon interactions. It is noteworthy that these lines will usually be subject to small (bathochromic) frequency shifts, which are not part of this analysis; in the present context, their value will be to assist the primary identification of local media effects. The second is the

appearance of entirely new lines in the Raman spectrum, resulting from vibrations that are allowed by different selection rules; those associated with three-photon (hyper-Raman[34]) or even four-photon interactions.

Order of magnitude estimates for the size of these effects can be obtained on the basis of simple assumptions, such as transition polarizability volumes $\alpha' = \alpha/4\pi\varepsilon_0$ whose values are comparable to molecular size. This, in turn, suggests that each additional vertex in a pair-interaction time-ordered diagram conveys a correction of the order of molecular size divided by the cube of the pair separation. On this basis, one can anticipate that sufficiently close molecules might exhibit new lines of comparable intensity to normal Raman bands. In principle, the modification to the symmetry of the molecule undergoing a change in vibrational state could be assisted by not just one but other additional molecules too; however, this would not elicit any further transitions beyond those arising from a nearest neighbor, as introduced in Subsections II D and II E.

The analysis has also highlighted a high order dependence of the newly emerging Raman lines on the isothermal compressibility. Since this signifies a strongly nonlinear dependence on pressure, there is additional scope to identify the responsible vibrations. It is nonetheless analysis of the associated, modified symmetry rules that will principally serve to fully characterize these modes.[35] Their detailed appraisal invites the introduction of irreducible tensor representations whose thorough analysis will be presented in a subsequent publication.

## ACKNOWLEDGMENTS

The authors would like to thank the University of East Anglia (UEA) and the Engineering and Physical Sciences Research Council for funding this research. We also thank Dr. Juan Antonio Rodriguez Ruiz (Universidad de Málaga), visiting scholar at UEA, for helpful comments.

[1]A. F. Chrimes, K. Khoshmanesh, P. R. Stoddart, A. Mitchell, and K. Kalantar-zadeh, Chem. Soc. Rev. **42**, 5880 (2013).
[2]A. F. Palonpon, M. Sodeoka, and K. Fujita, Curr. Opin. Chem. Biol. **17**, 708 (2013).
[3]K. A. Antonio and Z. D. Schultz, Anal. Chem. **86**, 30 (2014).
[4]R. S. Das and Y. K. Agrawal, Vib. Spectrosc. **57**, 163 (2011).
[5]C. Krafft and J. Popp, Anal. Bioanal. Chem. **407**, 699 (2014).
[6]D. Cialla, A. März, R. Böhme, F. Theil, K. Weber, M. Schmitt, and J. Popp, Anal. Bioanal. Chem. **403**, 27 (2012).
[7]E. C. L. Ru and P. G. Etchegoin, Annu. Rev. Phys. Chem. **63**, 65 (2012).
[8]Z. H. Kim, Front. Phys. **9**, 25 (2013).
[9]S. Schlücker, Angew. Chem., Int. Ed. **53**, 4756 (2014).
[10]Y. S. Yamamoto, Y. Ozaki, and T. Itoh, J. Photochem. Photobiol. C **21**, 81 (2014).
[11]E. L. Keller, N. C. Brandt, A. A. Cassabaum, and R. R. Frontiera, Analyst **140**, 4922 (2015).
[12]L. Rodriguez-Lorenzo, L. Fabris, and R. A. Alvarez-Puebla, Anal. Chim. Acta **745**, 10 (2012).
[13]H. Wang, X. Jiang, S.-T. Lee, and Y. He, Small **10**, 4455 (2014).
[14]L. Yang, P. Li, and J. Liu, RSC Adv. **4**, 49635 (2014).
[15]D.-W. Li, W.-L. Zhai, Y.-T. Li, and Y.-T. Long, Microchim. Acta **181**, 23 (2013).
[16]Z. Li, M. J. Deen, S. Kumar, and P. R. Selvaganapathy, Sensors **14**, 17275 (2014).
[17]S. McAughtrie, K. Faulds, and D. Graham, J. Photochem. Photobiol. C **21**, 40 (2014).
[18]D. P. Craig and T. Thirunamachandran, *Molecular Quantum Electrodynamics: An Introduction to Radiation-Molecule Interactions* (Dover Publications, Mineola, NY, 1998).
[19]G. Juzeliūnas, Phys. Rev. A **53**, 3543 (1996).
[20]D. L. Andrews and D. S. Bradshaw, Eur. J. Phys. **25**, 845 (2004).
[21]A. Salam, *Molecular Quantum Electrodynamics: Long-Range Intermolecular Interactions* (Wiley, Hoboken, NJ, 2010).
[22]D. L. Andrews and D. S. Bradshaw, Ann. Phys. (Berlin) **526**, 173 (2014).
[23]D. L. Andrews and N. P. Blake, Phys. Rev. A **41**, 2547 (1990).
[24]D. L. Andrews, D. S. Bradshaw, J. M. Leeder, and J. Rodríguez, Phys. Chem. Chem. Phys. **10**, 5250 (2008).
[25]L. Mandel and E. Wolf, *Optical Coherence and Quantum Optics* (Cambridge University Press, Cambridge, NY, 1995).
[26]J. A. Salthouse and M. J. Ware, *Point Group Character Tables and Related Data* (Cambridge University Press, London, 1972).
[27]M. P. E. Lock, D. L. Andrews, and G. A. Jones, J. Chem. Phys. **140**, 044103 (2014).
[28]See supplementary material at http://dx.doi.org/10.1063/1.4948366 for the complete molecular tensor expressions.
[29]L. C. Dávila Romero, S. Naguleswaran, G. E. Stedman, and D. L. Andrews, Nonlinear Opt. **23**, 191 (2000).
[30]D. L. Andrews and T. Thirunamachandran, J. Chem. Phys. **67**, 5026 (1977).
[31]D. H. Friese, M. T. P. Beerepoot, and K. Ruud, J. Chem. Phys. **141**, 204103 (2014).
[32]C. D. Allemand, Appl. Spectrosc. **24**, 348 (1970).
[33]D. A. Long, *The Raman Effect: A Unified Treatment of the Theory of Raman Scattering by Molecules* (Wiley, Chichester, New York, 2002).
[34]D. L. Andrews and T. Thirunamachandran, J. Chem. Phys. **68**, 2941 (1978).
[35]D. L. Andrews and P. Allcock, *Optical Harmonics in Molecular Systems* (Wiley-VCH, Weinheim, 2002).